AD-A166 545 STRUCTURAL INELASTICITY (28TH) A FINITE ELEMENT 1/1
'VECTORIZATION' METHOD FO. (U) MINNESOTA UNIV
MINNEAPOLIS DEPT OF AEROSPACE ENGINEERING AND M.
UNCLASSIFIED P G HODGE FEB 86 AEM-H2-4 N00014-82-K-0020 F/G 20/11 NL

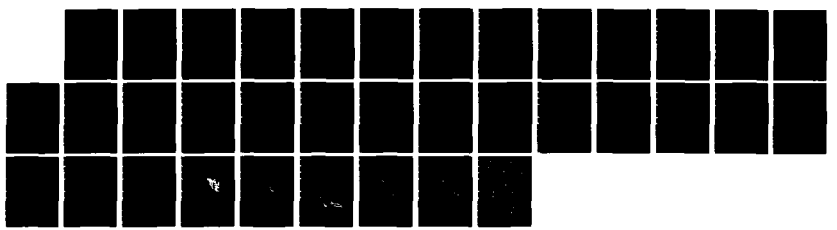

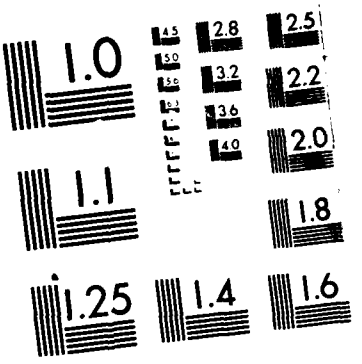

MICROCOPY RESOLUTION TEST CHART

AD-A166 545

Report AEM-H2-4

STRUCTURAL INELASTICITY XXVIII

Final Report on A Finite Element "Vectorization" Method for the Solution of Crack Growth Problems in two or three Dimensions

Philip G. Hodge, Jr., Professor of Mechanics

Department of Aerospace Engineering and Mechanics
University of Minneosta
Minneapolis, Minnesota 55455

February, 1986

Final Report

~~Qualified requesters may obtain copies of this report from DDC~~

Prepared for

OFFICE OF NAVAL RESEARCH
Arlington, VA 22217

OFFICE OF NAVAL RESEARCH
Chicago Branch Office
536 South Clark St.
Chicago, IL 60605

DTIC FILE COPY

DTIC
ELECTE
APR 14 1986
S
E

This document has been approved for public release; its distribution is unlimited.

86 2 21 034

SECURITY CLASSIFICATION OF THIS PAGE (When Data Entered)

REPORT DOCUMENTATION PAGE	READ INSTRUCTIONS BEFORE COMPLETING FORM
1. REPORT NUMBER: AEM-H2-4	2. GOVT ACCESSION NO.: AD-A166545
	3. RECIPIENT'S CATALOG NUMBER:
4. TITLE (and Subtitle): Final Report	5. TYPE OF REPORT & PERIOD COVERED: Technical Report
	6. PERFORMING ORG. REPORT NUMBER:
7. AUTHOR(s): Philip G. Hodge, Jr., Prof. of Mechanics	8. CONTRACT OR GRANT NUMBER(s): N00014-82-K-0020
9. PERFORMING ORGANIZATION NAME AND ADDRESS: University of Minnesota, Minneapolis, Minnesota 55455	10. PROGRAM ELEMENT, PROJECT, TASK AREA & WORK UNIT NUMBERS: NF 064-429
11. CONTROLLING OFFICE NAME AND ADDRESS: OFFICE OF NAVAL RESEARCH, Arlington, VA 22217	12. REPORT DATE: February 1986
	13. NUMBER OF PAGES: 32
14. MONITORING AGENCY NAME & ADDRESS(if different from Controlling Office): OFFICE OF NAVAL RESEARCH, Chicago Branch Office, 536 South Clark St., Chicago, IL 60605	15. SECURITY CLASS. (of this report): Unclassified
	15a. DECLASSIFICATION/DOWNGRADING SCHEDULE:

16. DISTRIBUTION STATEMENT (of this Report)

~~Qualified requestors may obtain copies of this report from DDC.~~

17. DISTRIBUTION STATEMENT (of the abstract entered in Block 20, if different from Report)

18. SUPPLEMENTARY NOTES

19. KEY WORDS (Continue on reverse side if necessary and identify by block number)

Plasticity, Crack propagation, Finite-element method.

20. ABSTRACT (Continue on reverse side if necessary and identify by block number)

A summary and bibliography are presented of the investigations of structural inelasticity which were carried out at the University of Minnesota under the sponsorship of the Office of Naval Research during the period 1981-1985. Also included is a report on an investigation completed after expiration of the contract.

Pg. 1

DD FORM 1 JAN 73 1473 EDITION OF 1 NOV 65 IS OBSOLETE
S/N 0102-014-6601

SECURITY CLASSIFICATION OF THIS PAGE (When Data Entered)

DISCLAIMER NOTICE

THIS DOCUMENT IS BEST QUALITY PRACTICABLE. THE COPY FURNISHED TO DTIC CONTAINED A SIGNIFICANT NUMBER OF PAGES WHICH DO NOT REPRODUCE LEGIBLY.

FINAL REPORT

Research conducted under this contract included two distinct projects. The first was concerned with using simple truss models to illustrate certain critical aspects of nonlinear material behavior. Results obtained were issued in two reports listed as items 1 and 2 in the bibliography on page 2. This project was carried out by the Principal Investigator, Philip G. Hodge, Jr.

The other project was concerned with using a constant-strain finite element method to find complete solutions for the stress and displacement in a plate with a centered crack. This research was carried out by James Malone, Research Assistant,* under the joint direction of the Principal Investigator and of Professor Robert Plunkett. The elastic solution was obtained first; it was presented in the report listed as item 3 in the bibliography. The elastic/plastic solution was completed after the expiration of this contract. A description of this phase constitutes the main body of this Final Report; it is planned to submit the material for publication.

Keywords: Plasticity, Finite Elem... Anal...

* Now Dr. James Malone, Research Engineer, General Motors Laboratory, Warren, Michigan.

Accession For
NTIS CRA&I
DTIC TAB
Unannounced
Justification
By
Distribution/
Availability Codes
Dist | Special
A-1 | 23

QUALITY INSPECTED 3

BIBLIOGRAPHY

Report AEM-H2-1
Philip G. Hodge, Jr.
SIMPLE EXAMPLES OF COMPLEX PHENOMENA IN PLASTICITY
"Mechanics of Material Behavior", R. T. Shield & G. Dvorak, eds., Elsevier Sci. Publ. Co., Amsterdam, 1984, pp147-173.

Report AEM-H2-2
Philip G. Hodge, Jr.
SIMPLE EXAMPLES OF NON-LINEAR TRUSS BEHAVIOR
International Journal of Solids and Structures, **20**, 1001-1008 (1984).

Report AEM-H2-3
James G. Malone, Philip G. Hodge, Jr., and Robert Plunkett
FINITE ELEMENT MESH FOR A COMPLETE SOLUTION OF A PROBLEM WITH A SINGULARITY
Journal of Computers and Structures (in press)

AN ELASTIC - PLASTIC FINITE ELEMENT SOLUTION FOR A CRACKED PLATE

by

Phillip G. Hodge, Jr., James G. Malone, Robert Plunkett

ABSTRACT

In this paper, the finite element method is applied to a center-cracked plate subject to opening mode tensile loading. A complete elastic-plastic plane-stress solution for strain hardening materials obeying a Von Mises yield condition and Prandtl-Reuss stress-strain relations is obtained using only constant strain elements. An accurate representation of the stress-strain field, even at distances very close to the crack tip, is achieved by the use of a mesh arrangement in which the size of the elements decreases in a geometric series as the crack tip is approached. The numerical solution is compared with and used to discuss the range of validity of the well known HRR (Hutchinson-Rice-Rosengren) crack tip solution valid for small scale yielding. The influence of different amounts of hardening and the effect of changes in the mesh arrangements are also considered. Features of the finite element algorithm which reduce the total computing time are discussed. The finite element program is executed on the Cray-1 computer and the effect of vectorization on computational speed is discussed for this problem.

1. INTRODUCTION.

In a recent paper [1] we have shown, for the particular problem of a center-cracked elastic plate under tensile loading, that a finite element formulation which uses only constant-strain elements can provide an accurate representation of the stress-strain field even in the neighborhood of the stress and strain singularities at the crack-tip. This was achieved by using a large number of triangular elements arranged in a mesh in which the size of the elements decreases in a geometric series as the crack tip is approached. The present paper extends this technique to handle nonlinear material behavior and discusses the resulting complete elastic-plastic solution for crack problems.

Methods commonly used in nonlinear finite element analysis are discussed by Bathe [2] and Zienkiewicz [3]; practical procedures for various applications have been presented by Bathe and Cimento [4] and also by Bergan et al [5]. In an elastic-plastic finite element analysis, the most effective way of dealing with the material nonlinearity is by an incremental approach in which the load is applied in a number of small increments. Within each increment, the true stress-strain relations are approximated and an iterative process is applied to ensure that the equilibrium equations are satisfied to within some specified level of accuracy. At each iterative step the solution of a banded system of linear algebraic equations is required which accounts for a large portion of the computational cost. For a given finite element mesh, the accuracy of the solution can be improved by reducing the size of the load increments and/or imposing a tighter convergence criterion. However, this may cause a substantial increase in the total computing time so that in practice a balance has to be struck between accuracy and computational cost.

Access to a CRAY-1 supercomputer has made it feasible for us to consider a technique for nonlinear finite element analysis which uses a large number of unknowns and many small load increments. This is possible because the computational speed and memory capacity of this machine are much greater than previous generations of computers. For example, rates of 69 MFLOPS (million floating point operations per second) have been recorded [6,7] on the CRAY-1S for the solution of dense systems of linear equations of order 300 using LU decomposition with pivoting (without resorting to the use of assembly language). This is about 28 times faster than the IBM 3033 and 600 times faster then the VAX 11/780. Rates in excess of 140 MFLOPS have been achieved by the use of assembly language [8].

In this paper, we consider the particular problem of a center-cracked plate subject to mode-1 (tensile opening mode) loading. Small strains and displacements are assumed. This means that material nonlinearities but not geometric nonlinearities are considered. This problem has been the subject of considerable interest. In the following we will mention only some of the many analytic and numerical papers which have appeared in the literature. A more detailed account is contained in the review article by Rice [9].

The asymptotic form of the plastic crack tip stress-strain field in plane strain and plane stress has been established analytically by Rice [10], Rice and Rosengren [11], and Hutchinson [12, 13] for strain hardening and perfectly plastic materials. This solution, frequently referred to as the HRR solution, is based on the deformation theory of plasticity and is valid under conditions of small scale yielding [14]. It will be discussed in more detail later in this paper.

For power law hardening materials, Tracey [15] used the finite element method to determine the plane-strain stress state at the tip of a crack under conditions of small scale yielding. He used special singularity elements at the crack tip in which the displacement shape functions were chosen to represent the form of the HRR solution; elsewhere 4-noded isoparametric elements were used. Hilton and Hutchinson [16], carried out a plane-stress finite element analysis for both small and large scale plastic yielding. Their method used constant strain triangular elements together with a special singular element surrounding the crack tip in which the HRR solution was embedded.

We have recently shown [1], for an elastic analysis, that constant strain elements can be used to obtain an accurate representation of the stress-strain field in the region near the crack tip. For the elastic-plastic analysis, our approach has also been to use a large number of constant strain triangular elements and a mesh which is similar to that used in the elastic finite element analysis [1]. Our nonlinear finite element procedure yields a complete elastic-plastic solution at a reasonable computational cost when executed on the CRAY-1. We demonstrate that on a scale in which the crack length equals one it is possible to obtain a sufficiently accurate solution for the stress field at distances as close as 10^{-6} from the crack tip. This solution is used to discuss both the spatial range over which the HRR solution holds and the level of applied load at which the HRR solution no longer accurately represents the crack tip stress-strain field. Our solution provides a good representation of the stress-strain field at all levels of applied load.

In section 2, we describe the element mesh and the algorithm which implements our elastic-plastic finite element analysis. The numerical results are discussed in Section 3. The effect of different element meshes on the computed solution and the

influence of hardening are also reported in that section. In Section 4, computing times for different meshes and for different amounts of hardening are discussed. Features of the algorithm including vectorization which reduce the computational cost are also described. Finally, some conclusions are presented in Section 5.

2. METHOD OF SOLUTION.

In this paper, the particular problem of a rectangular plate containing a centrally located crack subject to mode-I (opening mode) loading is considered. The crack length is 2a and the plate is of height 2h and width 4a (see Fig. 1). The boundary conditions along the top and bottom edges are uniform displacements in the vertical direction and zero traction components in the horizontal direction. Zero tractions are prescribed on the remaining edges of the plate and along the crack faces SG. By the usual symmetry argument, the problem can be reduced to that of solving for one quadrant ABEF (shaded area) of the plate with boundary conditions as shown in Fig. 1.

(a) Finite element mesh.

The finite element program is based on the well known displacement method and uses only constant strain elements. The rectangular domain ABEF (Fig. 1) is discretized into triangular elements by a mesh generating program which has been developed so that different mesh arrangements can be automatically produced. A typical mesh arrangement using 216 elements is shown in Fig. 2. Meshes ranging in size from 564 to 2064 elements and having elements as small as 10^{-6} a at the crack tip have been used in this study.

The mesh over portion ABCD of the plate is formed from the quadrilaterals defined by a set of rectangular rings intersected by rays. Let M numbers r_i be defined by

$$r_M = a, \quad r_i = \alpha r_{i+1}, \qquad i=M-1,M-2,\ldots 2,1 \qquad (2.1)$$

where α is a constant. The rings are a set of nested $r_i \times 2r_i$ rectangles with lower corners along AGB (see Fig. 2) at distances $\pm r_i$ from the crack tip G. Let N-1 equidistant points be inserted along BC and the same spacing continued along CD and DA. The rays are straight lines from G through these points. The innermost ring is divided into $4N^2$ equal iscosceles triangles and the quadrilaterals in the remaining rings are each split into two triangles by their diagonals as shown in Fig. 2. Finally the mesh is completed by filling the remaining portion DCEF with approximately square rectangles of constant size which are split into triangles. The mesh shown in Fig. 2 is for M=5 and N=3.

The aspect ratio F of a generic triangle JKL in ring i+1 along GB is given by

$$F = |JK|/|JL| = (r_{i+1} - r_i)/(r_i/N) = N[1/\alpha - 1] \qquad (2.2)$$

Hence the geometric coefficient α in Eq (2.2) is related to a typical aspect ratio by

$$\alpha = (1+F/N)^{-1} \qquad (2.3)$$

We have found that good results are obtained by taking F=1.

A similar mesh has been used [1] in an elastic study of an infinite plate containing a centrally located crack. The main features of this mesh arrangement are more fully

discussed in Ref. [1].

(b) Material properties.

The plate material is assumed to be homogeneous and initially isotropic, obeying Hooke's law in the elastic range with initial yielding determined by the Von Mises yield condition. After yielding, plastic strain increments are defined by an associated flow rule with linear hardening. Isotropic growth of the yield condition is assumed. At any point where unloading occurs the incremental form of Hooke's law will again apply. These assumptions lead to the well known Prandtl-Reuss stress-strain relations in the incremental theory of plasticity. The solution presented in this paper is for a state of plane-stress. It is also assumed that both strains and rotations are small. The validity of these assumptions will be discussed in Section 3.

The elastic-plastic stress-strain matrix $D(\sigma)$ which relates changes in stress to changes in strain at points of the material which have yielded and are loading has been derived under the above assumptions by Yamada et al [17]. During any time increment Δt the stress increments $\Delta\sigma$ and strain increments $\Delta\epsilon$ are related by

$$\Delta\sigma = D(\sigma)\,\Delta\epsilon \qquad (2.4)$$

where $\Delta\sigma = [\Delta\sigma_x\ ,\ \Delta\sigma_y\ ,\ \Delta\tau_{xy}\ ]^T$, $\Delta\epsilon = [\Delta\epsilon_x\ ,\ \Delta\epsilon_y\ ,\ \Delta\gamma_{xy}\ ]^T$, and γ_{xy} is the engineering shear component of strain. If the material is elastic, $D(\sigma)$ is the constant matrix

$$D(\sigma) = D_E \equiv E/(1-\upsilon^2)\begin{bmatrix} 1 & \upsilon & 0 \\ \upsilon & 1 & 0 \\ 0 & 0 & (1-\upsilon)/2 \end{bmatrix} \qquad (2.5)$$

whether or not earlier plastic behavior has taken place. If it is plastic,

$$D(\sigma) = D_{EP} \equiv (E/Q)\begin{bmatrix} \sigma_y'^2 + 2P & -\sigma_x'\sigma_y' + 2\upsilon P & -\tau_{xy}(\sigma_x' + \upsilon\sigma_y')/(1+\upsilon) \\ -\sigma_x'\sigma_y' + 2\upsilon P & \sigma_x'^2 + 2P & -\tau_{xy}(\sigma_y' + \upsilon\sigma_x')/(1+\upsilon) \\ -\tau_{xy}(\sigma_x' + \upsilon\sigma_y')/(1+\upsilon) & -\tau_{xy}(\sigma_y' + \upsilon\sigma_x')/(1+\upsilon) & R/2(1+\upsilon) + (2H/9E)(1-\upsilon)\,\bar{\sigma}^2 \end{bmatrix} \qquad (2.6)$$

where σ' is the deviatoric stress and $\bar{\sigma}$ is the equivalent stress.

$$\bar{\sigma} = [(3/2)(\sigma'_{ij}\sigma'_{ij})]^{1/2}$$

$$P = (2H/9E)\,\bar{\sigma}^2 + \tau_{xy}^2\,/(1+\upsilon)$$

$$Q = R + 2(1-\upsilon^2)P \qquad (2.7)$$

$$R = \sigma_x'^2 + 2\upsilon\sigma_x'\sigma_y' + \sigma_y'^2$$

$$H = EE_T/(E-E_T)$$

where υ is the Poisson's ratio, E is Young's Modulus, and E_T is the plastic modulus.

A plot of equivalent stress $\bar{\sigma}$ versus equivalent strain $\bar{\epsilon}$ for a material satisfying our constitutive assumptions is shown in Fig. 3. The equivalent strain $\bar{\epsilon}$ is defined as

$$\bar{\epsilon} = [(3/2)(\epsilon'_{ij}\,\epsilon'_{ij})]^{1/2} \qquad (2.8)$$

where ϵ'_{ij} are the deviatoric components of strain. In practice a piecewise linear stress-strain law can be determined from data obtained by a simple tension test for a real material. We have chosen the most simple case, i.e. a bilinear stress-strain law, but the above discussion can be modified in an obvious manner to handle any piecewise linear curve.

(c) Nonlinear finite element analysis.

Since the strain is constant in each element, the column matrix of element strains ϵ and the column matrix of nodal displacements u are related by

$$\epsilon = B\,u \qquad (2.9)$$

where the constant matrix B depends only on geometry and not on material behavior.

The nodal force matrix F and the stress matrix σ are related by the similar relation

$$F = A\,\sigma \qquad (2.10)$$

where A also depends only on geometry. Equations (2. 9) and (2. 10) must be valid for either total or incremental behavior.

During any incremental time step Δt, the stress and strain increments are related by

$$\Delta\sigma = \int_{\epsilon}^{\epsilon+\Delta\epsilon} D(\sigma)\,d\epsilon = D(\sigma^*)\,\Delta\epsilon \qquad (2.11)$$

where σ^* is some mean value of the stress state during the strain interval $\Delta\epsilon$.
Combining Eqs, (2. 4), (2. 9), and (2. 10) we obtain the usual matrix equation

$$K(\sigma)\Delta u = \Delta F \qquad (2.12)$$

where the "stiffness" matrix K is given by

$$K(\sigma) = A\,D(\sigma)\,B \qquad (2.13)$$

Due to the incremental nature of the stress-strain relations (see Eq. (2. 11)), this problem is best solved by an incremental procedure in which the load is applied in a

series of increments ΔF_M. Thus the load at the end of increment M is

$$F_M = F_{M-1} + \Delta F_M , \qquad M=1,2,\ldots,q \qquad (2.14)$$

where F_0, F_q are the initial and final loads respectively.

The problem can be posed as follows: Given a complete solution u_{M-1}, ϵ_{M-1}, σ_{M-1} at the end of the $(M-1)^{th}$ step corresponding to the applied external load F_{M-1}, find the complete solution u_M, ϵ_M, σ_M at the end of the M^{th} step corresponding to the external load F_M. By a complete solution, we mean column matrices for nodal displacements, nodal forces, element strains, and element stresses. The process during the M^{th} step is to obtain incremental changes Δu_M, $\Delta \epsilon_M$, $\Delta \sigma_M$ in displacements, strains, and stresses, respectively, corresponding to the increment in load ΔF_M which satisfy Eqs. (2.9) to (2.11), i.e.

$$\Delta \epsilon_M = B \Delta u_M \qquad (2.15)$$

$$\Delta \sigma_M = D(\sigma_M^*)\, \Delta \epsilon_M \qquad (2.16)$$

$$F_M = A \sigma_M \qquad (2.17)$$

where $\sigma_M = \sigma_{M-1} + \Delta \sigma_M$ and σ_M^* is some mean value of the stress state during the strain interval $\Delta \epsilon_M$ (σ_M^* will be defined later).

The first step is fully elastic and the solution is obtained by direct solution of the elastic finite element equations. For each later step an iterative method is used to solve the kinematic, constitutive, and equilibrium equations (2.15, -16, -17) at step M. The first estimate $\Delta u_M^{(1)}$ is given by

$$\Delta u_M^{(1)} = \Delta u_{M-1} \qquad (2.18)$$

where Δu_{M-1} is the change in displacement which occurred during the previous $(M-1)^{th}$ step. Next $\Delta \epsilon_M^{(1)}$ and $\Delta \sigma_M^{(1)}$ are obtained in order from Eqs. (2.15) and (2.16) using σ_{M-1} as the initial mean stress $\sigma_M^{*(1)}$; the first total stress estimate $\sigma_M^{(1)}$ is obtained by adding $\Delta \sigma_M^{(1)}$ to the initial value σ_{M-1}.

In general $\sigma_M^{(1)}$ will not satisfy equilibrium. We begin the iterative process by defining a residual force:

$$P_M^{(1)} = F_M - A \sigma_M^{(1)} \qquad (2.19)$$

and obtain a correction to the displacement increment field by solving

$$K_M\, \delta u_M^{(1)} = P_M^{(1)} \qquad (2.20)$$

where

$$K_M = A\, D(\sigma_{M-1})\, B \qquad (2.21)$$

K_M is factored (Cholesky algorithm) in the first iteration. This factored form is thereafter retained for the current step so that only a back-substition need be performed to solve (2.20) for each succeeding iteration. Then $\Delta u_M^{(2)}$ is obtained by adding $\delta u_M^{(1)}$ to $\Delta u_M^{(1)}$ and $\Delta \epsilon_M^{(2)}$ is obtained from (2.15). A mean stress σ_M^*

(2) is defined by

$$\sigma_M^{*(2)} = (\sigma_{M-1} + \sigma_M^{(1)})/2 \qquad (2.22)$$

and $\Delta\sigma_M^{(2)}$ is then given by (2. 16).

This iterative process is repeated until the residual forces $P_M^{(i)}$ at the i^{th} iteration satisfy

$$|| P_M^{(i)} || < TOL \qquad (2.23)$$

where $|| P_M^{(i)} ||$ is the magnitude of the largest component (in absolute value) of $P_M^{(i)}$ over all the nodes and TOL is some preset convergence tolerance.

The iterative procedure at the M^{th} step can be summarized in the following algorithm:

$$\begin{aligned}
&\Delta u_M^{(i+1)} = \Delta u_M^{(i)} + \delta u_M^{(i)} \\
&\Delta \epsilon_M^{(i+1)} = B\, \Delta u_M^{(i+1)} \\
&\sigma_M^{*(i+1)} = (\sigma_{M-1} + \sigma_M^{(i)})/2 \\
&\sigma_M^{(i+1)} = \sigma_{M-1} + D(\sigma_M^{*(i+1)})\, \Delta \epsilon_M^{(i+1)} \\
&P_M^{(i+1)} = F_M - A\, \sigma_M^{(i+1)} \\
&K_M\, \delta u_M^{(i+1)} = P_M^{(i+1)}
\end{aligned} \qquad (2.24)$$

where $\delta u_M^{(0)} = 0$, $\Delta u_M^{(0)} = \Delta u_{M-1}$, $\sigma_M^{(0)} = \sigma_{M-1}$ and i= 0,1,2,3, ... It can be seen that this approach is a modified form of the Newton-Raphson method for solving a non-linear system of equations (see Refs. [2, 3]).

(d) Load step size.

One of the advantages of using constant strain elements is that at any given applied load the stress throughout each element will be constant. Further for the problem considered here, no unloading of yielded elements occurs. Therefore, at any given load each element is either elastic and has never yielded or is plastic and loading. Our numerical procedure is to terminate a load step when any elastic element reaches yield. When this procedure is used each element will remain either elastic or plastic throughout the entire load step.

Since any single iteration is a strictly linear process, the load F_M at which the M^{th} step is terminated can be easily estimated in the following way. At the beginning of the M^{th} load step we apply some arbitrary load increment ΔF_M and proceed to compute $\Delta u_M^{(1)}$, $\Delta \epsilon_M^{(1)}$, $\Delta\sigma_M^{(1)}$ in the manner described above. Then for each elastic element β we compute a scalar factor $\gamma_{M\beta}^{(1)}$ which satisfies

$$\bar{\sigma}^2(\sigma_{M-1\,\beta} + \gamma_{M\beta}^{(1)} \Delta\sigma_{M\beta}^{(1)}) = Y_\beta^2 \qquad (2.25)$$

where Y_β is the initial yield stress. Based on the stress change $\Delta\sigma_M^{(1)}$ we predict that the element α for which

$$\gamma_{M\alpha}^{(1)} = \min_{\beta} \{ \gamma_{M\beta}^{(1)} \} \qquad (2.26)$$

will be the element most likely to first reach yield during the current load step. The entire incremental solution can now be scaled by the factor $\gamma_{M\alpha}^{(1)}$

$$\Delta\sigma_M^{(1)} = \gamma_{M\alpha}^{(1)} \Delta\sigma_M^{(1)} \qquad (2.27)$$

so that element α will have just reached yield when the load is incremented by an amount

$$\Delta F_M = \gamma_{M\alpha}^{(1)} \Delta F_M \qquad (2.28)$$

At each iteration, improved estimates of the load increment ΔF_M required to have element α just reach yield can be obtained by computing scaling factors $\gamma_{M\alpha}^{(i)}$ for element α corresponding to the stress change $\Delta\sigma_{M\alpha}^{(i)}$ using Eq.(2.25).

It was found that computing scaling factors for only the first three iterations in each load step was the most efficient procedure. The load increment ΔF_M is then held fixed for the remaining iterations of the load step. At the end of the load step, the yield condition may not be satisfied exactly by element α but this is taken care of by the use of a "smeared" yield condition.

The idea of a smeared yield condition is based on a technique used by Yamada et al [17] and, in a different context, by Hodge and Van Rij [18, 19] to substantially reduce the total number of load steps. At the end of each load step, any elastic element β for which the equivalent stress $\bar{\sigma}$ satisfies

$$0.99\, Y_\beta < \bar{\sigma} < 1.02\, Y_\beta \qquad (2.29)$$

has its yield stress Y_β redefined so that $Y_\beta = \bar{\sigma}$.

This means that elements which have not yet reached yield but which are close enough to satisfy (2.29) can be treated as plastic in the next step. This avoids the need for one or more additional steps to bring these elements to yield. It also means that the solution at the end of the step can be accepted even if some elements exceed the yield stress, provided (2.29) is satisfied. The alternative would be to repeat the load step using an improved estimate for the initial size of the load increment.

The main features of the program have been described above. A more detailed description of the program algorithm may be found in Ref [20] which contains the program documentation and Fortran code.

3. RESULTS AND DISCUSSION.

In this section an assessment of the accuracy of the solution particularly in the region close to the crack tip will be given. The effect of different mesh arrangements on the solution will also be discussed. Comparisons will be made between elastic-plastic solutions corresponding to different amounts of hardening and also with the purely elastic solution. The numerical elastic-plastic solution in the region surrounding the crack tip will be compared with an analytic solution which is valid under conditions of small scale yielding in which the plastic zone is small compared to the plate dimensions.

(a) Finite element solution.

The plate material has Young's Modulus E = 185.1 G Pa, Poisson's ratio υ = 0.3 , initial yield stress Y = 225.4 M Pa, and obeys a bilinear stress-strain law with plastic modulus E_T =2.372 G Pa. The plate dimensions are h=250 mm and a=75 mm (see Fig. 1). This particular geometry and material properties were selected so that the numerical solution could also be compared with the experimental results of Yagawa et al. [21].

They reported the increase of a gage length in a centrally cracked thin (5 mm thick) aluminum plate as a function of load. The gage points straddling the crack were located at distances of 80 mm directly above and below the center of the plate. Our finite element solution was obtained using mesh A (see Table 1) and agrees closely with the experiment as shown in Figure 4. A dimensionless load f has been defined by dividing by the initial yield load of the uncracked plate: f= F/A,Y where A_1 is the area of the top edge of the plate. Henceforth, " applied load " refers to f. Yagawa et al [21] found a gage point displacement of 4.43 mm at an applied load of 0.87 at which load the crack began to grow, whereas for the same displacement our numerical solution predicts an applied load of 0.93, which is 7% greater than the measured value.

The plastic zones at different levels of applied load are shown in Figs. 5 and 6. It can be seen that the overall shape of the plastic zone is somewhat influenced by the level of applied load. Our numerical results show that the plastic zone has a radius of about 0.1a in the region ahead of the crack tip at an applied load of 0.3 . The plastic zone first reaches the outer edge EF of the plate (see Fig. 1) when the applied load is 0.51 ; at this load the knee occurs in the load versus gage point displacement curve (Fig. 4). At a load of 0.6 the plastic zone covers about 15% of the area of the quadrant ABEF and extends to cover 60% of this area at a load of 0.9 .

The equivalent stress $\bar{\sigma}$ computed at an applied load of 0.3 along 5 rays radiating from the crack tip is plotted versus log (r/a) in Fig. 7 where r and θ are polar coordinates referred to the crack tip. The radial distance r is measured from the crack tip to the centroid of the element in which $\bar{\sigma}$ is computed. . Each curve displays a fairly abrupt kink indicated for example by the arrow in Fig. 7 for the ray $\theta = 168^0$. Along each ray the kink occcurs at the elastic-plastic boundary. The stresses drop off sharply over a short distance beyond the elastic-plastic boundary. Similar behavior is observed at other levels of applied load.

As the applied load increases above 0.5 and the plastic zone extends across the plate, it is found that the equivalent stresses in the region close to the crack tip ($r/a<10^{-2}$) are greater than but approximately proportional to the equivalent stresses obtained from the purely elastic solution. The factors of proportionality are about 2.6 and 1.4 at applied loads of 0.6 and 0.9, respectively. This means that, at applied loads greater than 0.5 the stress field displays a $1/\sqrt{r}$ singularity at the crack tip. The detailed behavior of the stress field at applied loads below f= 0.5 will be discussed later in subsection (d).

Figure 8 shows the ϵ_γ components of strain on a log-log scale. The strains along the 49^0 ray show a $1/\sqrt{r}$ variation at the crack tip over the range $r/a < 2.0 \times 10^{-3}$. Along this ray, the elastic-plastic boundary is located at r/a = 0.15. Over the range $r/a > 0.15$ the ϵ_γ strain components are greater than those which would be obtained from a purely elastic solution. For example, the percentage difference between the strains from the elastic-plastic and elastic solutions decreases from 10% just

outside the elastic-plastic boundary to less than 3% near the edge of the plate (for r/a > 0.9). As the applied load is increased the distance from the crack tip over which ϵ_y displays a $1/\sqrt{r}$ variation increases in extent up to a maximum distance of about r/a = 0.02 along the 49^0 ray at an applied load of 0.9. The behaviour of the strain along other rays is qualitatively similar; the largest ϵ_y strain components occur along the ray for which $\theta = 61^0$.

We have also considered a material with a higher amount of hardening (E_T = 18.51 G Pa). The behavior of the stress-strain field for this material is qualitatively similar to that obtained for the lower hardening material (E_T = 2.372 G Pa) which has been discussed above.

(b) Effect of different mesh arrangements.

The presence of a singularity in the stress-strain field at the crack tip requires that the arrangement of elements in the mesh must be carefully selected if an accurate solution is to be achieved at a reasonable computational cost. The elastic finite element solution for a crack problem, using a mesh similar to that described in Sec. 2 is discussed in Ref. [1]. It was found that increasing the number of rings in the mesh produced more accurate results in the region close to the crack tip, whereas an increase in the number of rays gave more accuracy over the rest of the plate. It was also shown that for a given mesh, increasing the number of rings while holding the number of rays fixed (thereby increasing the density of elements only at the crack tip) produced less than 0.1% improvement in the accuracy of the solution over the range $r > 100r_1$, where r_1 is the position of the innermost ring in the original mesh. We now show that similar observations hold for the elastic-plastic problem.

Four specific mesh arrangements have been considered (Table 1). Solutions for the high-hardening material (E_T =18.51 G Pa)were obtained for each mesh over a range of loads up to 0.9 . At this load the plastic zone extended to touch almost all of the edge EF (see Fig. 2). To facilitate a comparison with the results of Ref. [1] , we will compare the vertical components of displacement v at nodes along the crack face obtained from each mesh. Similar behavior is observed for v along other radial directions and also for the strain field.

Meshes A and B were chosen to study the effect of changing the number of rings while keeping the numbers of rays fixed. The solutions obtained from meshes A and B show no difference in v over the range $10^{-2} < r/a < 1$ at all levels of loading. However, over the range $10^{-4} < r/a < 10^{-2}$ the vertical displacements v obtained from mesh B are less than those obtained from mesh A. The difference between the two solutions increases as the crack tip is approached. For example, at an applied load of 0.3 the differences in v are appproximately 0.5%, 5.5%, and 16% at r/a equal to 10^{-3}, 10^{-4}, and 3.33×10^{-5} (the position of the node on the crack face adjacent to the crack tip in mesh B), respectively.

The effect of increasing the density of the elements over the entire plate by doubling the number of rays while holding the number of rings fixed, was studied by comparing meshes C and D. The vertical displacements v along the crack face obtained from the coarse mesh C are smaller than those obtained from the refined mesh D. For example, at an applied load of 0.3 the differences in v were approximately 1.4%, 2%, 3%, and 7% at r/a equal to 1, 10^{-1}, 10^{-2}, and 4.6×10^{-4}, respectively.

An assessment of the accuracy of the finite element solution for the elastic problem [1] was made possible by a comparison with an exact analytic solution. It

was found that the elastic strain and displacement fields obtained by the use of mesh A were in very good agreement with the analytic solution. For example, the error in vertical displacement v along the crack face was 2%, 4%, 6%, and 14% at r/a equal to 1, 10^{-2}, 10^{-4}, and 10^{-6}, respectively.

In the absence of a complete analytic solution for the elastic-plastic problem, it is not possible to determine the accuracy of the finite element solution directly, as was done for the elastic problem. However, the observations which have been made on the effect of different mesh arrangements for the elastic-plastic problem are qualitatively the same and in close quantitative agreement with those made in Ref.[1] for the elastic problem. Given this agreement, we can infer from the results of [1] that mesh A should also be expected to provide an element arrangement for which an accurate elastic-plastic solution can be obtained over the range $r/a > 10^{-6}$. This assertion is borne out later in the paper when the numerical solution is compared with the analytical HRR crack tip solution under conditions of small scale yielding.

For the elastic-plastic problem, it is found (see Section 5) that the computational cost increases by a factor of about 10 when the number of rays in the mesh is doubled (i.e. changing N=3 to N=6). However, from the elastic results [1], it would be expected that this change in the mesh would only slightly improve the accuracy of the solution, e.g. by approximately 1%, 2%, 3%, and 6% in v at r/a equal to 1, 10^{-2}, 10^{-4}, and 10^{-6}, respectively. It was concluded that mesh A can be expected to provide the best element arrangement in terms of balancing computational cost and accuracy over the range $r/a > 10^{-6}$ for the elastic-plastic analysis.

(c) Small scale yielding and the HRR solution.

The analytic crack tip HRR solution [10,11, and 12] is based on a deformation theory of plasticity and is valid under conditions of small scale yielding. The term small scale yielding refers to the situation in which the applied load is sufficiently low so that the size of the plastic zone is small compared to the length of the crack; it is small enough that the plastic zone is embedded in an elastic field governed by the dominant $1/\sqrt{r}$ term in the asymptotic elastic series solution. In obtaining the HRR solution, the $1/\sqrt{r}$ elastic term is the assumed boundary condition for large r. However, the HRR analysis cannot predict how large the plastic zone may become so that the $1/\sqrt{r}$ elastic term is still a good approximation for the solution in the region surrounding the plastic zone. Further, the HRR solution represents the elastic-plastic solution only over a small region of the plastic zone located at the crack tip. The extent of this region cannot be determined from the HRR analysis.

Our numerical results provide a solution over the entire plastic zone and are based on an incremental flow theory of plasticity. It has been shown [22] that a solution obtained using deformation theory will be similar to that obtained using an incremental flow theory of plasticity provided the condition of proportional stressing is satisfied. It has been pointed out [13] that proportional stressing can be expected to hold under the assumption of small scale yielding for a material obeying a bilinear stress-strain law.

For such a material Hutchinson [12] has shown that the radial and angular variation of the stresses in the HRR solution has the same form as the dominant term in the elastic solution. In the HRR solution the equivalent stress $\bar{\sigma}_{HRR}$ at a point (r, θ) can be represented by

$$\bar{\sigma}_{HRR} = Kr^{-1/2}[\cos^2(\theta/2) + (3/4)\sin^2\theta]^{1/2} \qquad (3.1)$$

where r and θ are polar coordinates referred to the crack tip. The amplitude K is given by

$$K = (E_T/E)^{1/2} K_I \qquad (3.2)$$

where K_I is the elastic stress intensity factor which replaces K in Eq. (3.1) to yield the elastic singular term.

Confidence in the accuracy of the numerical solution in the crack tip region can be gained from a comparison with the HRR solution. On the other hand, the accurate numerical solution can be used to assess the range over which the HRR solution is valid at different levels of applied load and also to determine the behavior of the solution over the remainder of the plastic zone in which the HRR solution does not hold. In addition, the level of applied load up to which the HRR solution provides an accurate description of the crack tip stress field can be estimated. These topics will be the subject of the discussion that follows.

(d) Comparison with the HRR solution for small scale yielding.

The elastic stress intensity factor K_I [used to compute $\bar{\sigma}_{HRR}$, see Eqs. (3.1) and (3.2)] has been determined from the elastic finite element solution by the method described in Refs. [1 and 23]. It has been shown [1] that K_I computed by this method will be accurate to within 3% of the correct value. For this problem, we have computed $K_I/\sqrt{a}\,Y = 1.23$. We compare the HRR and finite element solutions for the low hardening material by examining the ratio $\lambda = \bar{\sigma}_{HRR}/\bar{\sigma}$ along the 49^0 ray where $\bar{\sigma}$ is the equivalent stress obtained from the numerical solution. The results are shown in Fig. 9.

For the elastic finite element analysis we know, by considering the analytic solution for $\bar{\sigma}$ (given by the $1/\sqrt{r}$ elastic term in the region near the crack tip), that the error in $\bar{\sigma}$ increases as the crack tip is approached. The error is about 20% in those elements nearest the crack tip but is less than 15% for $r/a > 10^{-4}$. As discussed in subsection (b) above, similar behaviour regarding the accuracy of $\bar{\sigma}$ can be expected from the elastic-plastic finite element solution. As a result, we can be reasonably confident that the difference between $\bar{\sigma}$ and $\bar{\sigma}_{HRR}$ at points for which $\lambda < 0.8$ can not be caused solely by inaccuracy in the numerical solution. The HRR solution provides an accurate representation of the near tip stress field over the range $r/a < \rho$ where ρ is unknown. However, from Fig. 9 we can easily determine an upper bound on ρ by using the criterion that the HRR solution can be considered to represent the stress field only at points for which $\lambda > 0.8$.

By comparing the λ curves for f equal to 0.07, 0.22, and 0.3 in Fig. 9, it can be seen that ρ increases in magnitude as the applied load is increased. However, these curves show that the HRR solution represents the stress field only over a very small portion of the plastic zone. For example, at f= 0.3 the elastic-plastic boundary along the 49^0 ray is at r/a = 0.15 but the HRR solution is certainly not valid beyond $r/a = 10^{-3}$.

As the load is increased above 0.45, the numerical solution for the stress field at the crack tip begins to differ increasingly from the HRR solution. For example, consider the curve corresponding to f = 0.6. This is expected because the plastic zone has extended to the edge of the plate (see Fig. 5) so that it can no longer be regarded as embedded in an elastic field governed by the $1/\sqrt{r}$ term. Therefore, the small scale yielding conditions assumed for the HRR solution are no longer true at these higher

applied loads. From our numerical results we conclude, for this particular crack problem, that the HRR solution does not represent the stress field anywhere in the vicinity of the crack tip when the applied load f exceeds about 0.5. It can be seen from the curve for $f = 0.6$ that the stress field displays the $1/\sqrt{r}$ singularity over the range $r/a < 10^{-2}$ but its amplitude is no longer determined by K in Eq.(3. 2).

Similar behaviour is exhibited by the elastic-plastic solution for the high hardening material (E_T = 18.51 G Pa). For this material, it is found that the range over which the HRR solution represents the crack tip stress field is slightly larger in size than that found for the low hardening material at the same applied load.

(e) Validity of the small strain and small rotation assumptions.

The ϵ_r components of strain are shown in Figure 8 for the low- hardening material at an applied load of 0.3 . The strains along the 49^0 ray are greater than 0.1 over the range $r/a < 10^{-3}$. It is clear that the assumption of small strains is violated in the region near the crack tip. The rotations of the elements in this region are also large.

A formulation which accounts for large strains and large rotations would be a more appropriate model. However, in our discussion (subsection (b)) on the effect of the different meshes, it was shown that changes in the solution over the region near the crack tip do not produce significant changes in the region away from the crack tip. The large-strains are limited to a very small region at the crack tip. It might then be expected that a large strain formulation would not significantly alter the solution over much of the remainder of the plate.

The same conclusions cannot be drawn at higher levels of applied load, e.g. f= 0.5 or greater, for which the plastic zone has reached the outer edge of the plate. At these loads the region of large strains has increased in size (for example, $r/a < 10^{-2}$ at f= 0.6) to the extent that a large strain solution would be expected to differ from the small strain solution over much of the plate.

4. COMPUTING TIME AND VECTORIZATION.

In our finite element analysis, the use of a large number of degrees of freedom, many small load steps, and a tight convergence criterion is feasible because of the speed of the CRAY-1 computer. For example, a typical load step involves the solution of 1300 linear equations and requires about 30 iterations for convergence; the computations for such a step take only 1.2 c. p. u. seconds.

For both the low and the high hardening materials the size of the load increments when using mesh A ranged from $\Delta f = 10^{-4}$ at lower applied loads up to $\Delta f = 10^{-2}$ at higher loads. The tolerance used in the convergence criterion (2.23) was set at TOL= 10^{-9} and was held fixed for each load step. At this tolerance the solution for u, ϵ, σ and nodal forces F converged to 3 places of decimals.

Information about the computations performed using different meshes for both the low and high hardening materials is displayed in Table 2. For the same mesh, the total c. p. u. time for the low-hardening material is about twice that required for the high-hardening material. For a particular material, the number of iterations required per step is independent of the choice of mesh and is governed only by the amount of nonlinearity present in the problem, i.e. on the extent of the plastic zone at the

current applied load. A comparison of the c.p.u. times for the high hardening material using meshes C and D shows that the computational cost is increased by a factor of about 10 when the density of elements over the entire plate is increased by a factor of 4.

An important feature of the CRAY-1 is its vector hardware which enables the machine to execute computational processes, in which the same arithmetic operation is performed on each element or pair of elements from an ordered set, by "vectorization". Vectorized computations are performed at a significant increase in speed compared to the more conventional "scalar" mode in which computations are performed sequentially. Guidelines for writing FORTRAN programs which make efficient use of vectorization can be found in Refs. [24-26].

In an experiment, vectorization was temporarily turned off for a run using mesh A so that vector and scalar speeds could be compared for our code. The computations involved in Eqs. (2. 15), (2. 16), (2. 17), and (2. 22) were carried out by vectorization at speeds which were 3, 5, 7, and 10 times greater, respectively, than those attained in scalar mode. Assembly of the global stiffness matrix and load column matrix is an inherently scalar process, the small amount of vectorization which could be achieved resulted in speeds which were only 1.5 times faster than scalar mode.

It is common [2,3], when using a modified Newton-Raphson scheme, to obtain an initial guess $\Delta u_M^{(1)}$ for the change in displacement during the M^{th} step by solving for $\Delta u_M^{(1)}$ from

$$K_M \Delta u_M^{(1)} = \Delta F_M \qquad (4.1)$$

However, in our algorithm, the initial guess $\Delta u_M^{(1)}$ is given by the displacement increment Δu_{M-1} from the previous step (see Eq. 2. 18). We found that this simple change substantially reduced the number of iterations required for convergence in each step. As a result the total c. p. u. time was reduced by a factor of about 2.

In the modified Newton-Raphson iterative scheme which we have discussed in Section 2, the stiffness matrix K is updated (using the current state of stress) at the beginning of each load step. An alternative is only to update K periodically and to retain the same factored form ($R^t R$ Cholesky algorithm) for a number of load steps. For this problem, we experimented with a periodic updating strategy based on the rate of convergence of the iterative process. However, we found that this strategy was difficult to implement successfully in our program. For example, our best attempts reduced the total computing time by at most 20% whereas for other meshes the same strategy actually increased the computing time. It was decided to retain the more simple algorithm (see Section 2) in which K is updated at the beginning of each load step (the computing times shown in Table 2 are for that algorithm).

For both materials 60% of the total computing time was involved in equation solving. In our program, the banded system of linear equations is solved by vectorized versions of the LINPACK routines SPBCO and SPBFA, available through the CRAY $SCILIB library.

5. CONCLUSIONS.

An elastic-plastic finite element method which uses only constant strain triangular elements has been developed for a problem which exhibits a stress singularity. The method yields a complete solution for stress, strain, and

displacement which is accurate even at points which are very close to the singularity. The method does not require any *a priori* knowledge of the form of the singularity. The load is applied in a series of small increments. The size of each increment is determined by the load at which the next element (out of all those that are currently elastic) is predicted to reach yield. The nonlinear material behavior is accounted for by a modified Newton-Raphson iterative process which ensures that the equilibrium equations are satisfied at the end of each load increment. The solution for the particular problem of a centrally cracked plate under tensile loading in a state of plane-stress has been presented.

The finite element solution was obtained by using a mesh in which the size of the elements decreases in a geometric series as the crack tip is approached (see Sec. 2). In section 4, it was shown that the effect of different element arrangements on the elastic-plastic solution is similar to that observed for the purely elastic solution (Ref.[1]). Features are included in the finite element algorithm which significantly reduce the total c.p.u. time. In addition, the finite element code was written to take advantage of the vectorizing capabilities of the CRAY-1 computer, thereby substantially decreasing the computational cost. A mesh was chosen, for our particular problem, which provided the best balance between accuracy and computational cost.

Confidence in the accuracy of the solution was gained from a comparison with the analytic HRR (Hutchinson-Rice-Rosengren) [10,11, and 12] solution in the neighborhood of the crack tip under conditions of small-scale yielding. It was shown that the HRR solution represents the behavior of the crack tip stress-strain field provided the applied average stress does not exceed about one half of the yield stress. Under conditions of small-scale yielding, the HRR solution characterized the stress-strain field in the vicinity of the crack tip only over a very small portion of the plastic zone located at the crack tip.

The method presented here could easily be extended to materials which obey a piecewise linear stress-strain law. Yield conditions other than Von Mises could also be considered. Other fracture problems such as edge cracks, non-uniform loading, shear loading, cracks in bending, etc. could all be trivially handled by changing the boundary conditions. For these problems, the influence of geometry and boundary conditions on the HRR solution could be studied. This has applications in determining minimum size requirements for specimens used to establish a "one parameter" fracture criterion based on the J-integral. The method could be modified to deal with cracks in inhomogeneous and/or anisotropic materials such as composites.

The method could also be extended, admittedly not without some effort, to study the state of stress at the tip of a growing crack for which the form of the singularity is not well understood in most materials. In a broader context, problems involving other forms of singularity such as point loads and reentrant corners could also be considered.

In this paper, the emphasis has been on showing that a finite element method which uses only constant strain elements can provide a complete elastic-plastic solution for a state of plane-stress even in the region of high stress gradient close to the singularity. However for real plates the state of stress in the vicinity of the crack tip is fully three dimensional. The plane-stress solution can be expected to hold only at distances from the crack tip which exceed the plate thickness. This means, for the particular geometry which we have considered, that the solution can have physical meaning only over a range of about $r/a > 0.05$. As discussed in Section 3(b), accurate

solutions can be obtained over this range using a coarse mesh (about 600 elements) in relatively small c. p. u. times. It has been shown (Sec. 3(e)) that large strains and rotations are predicted in a neighborhood surrounding the crack tip, the size of which increases as the applied stress is increased. The assumption of small strains over the range $r/a > 0.05$ holds only when the applied stress is less than half the yield stress.

This suggests that a three dimensional finite element analysis with a formulation to account for large strains and rotations is required to obtain a better understanding of the fracture process in the region close to the crack tip. The nonlinear finite element algorithm and mesh ideas introduced here could be extended to the three dimensional problem using constant strain tetrahedral elements. The increased speed and memory capacity of the more recent models of the CRAY supercomputer make it reasonable to expect that a full three dimensional elastic-plastic solution can be achieved for this problem.

ACKNOWLEDGEMENT

The results presented in this paper were obtained with the support of the Office of Naval Research, the University of Minnesota Computer Center, and the Minnesota Supercomputer Institute. The authors also acknowledge the valuable assistance of Dr. C. C. Hsiung and his colleagues at Cray Research, Inc.

REFERENCES

1. J. G. Malone, P. G. Hodge, Jr., and R. Plunkett, Finite element mesh for a complete solution of a problem with a singularity, Computers and Structures, (in press).

2. K. J. Bathe, Finite Element Procedures in Engineering Analysis, Prentice-Hall, Inc. (1982).

3. O. C. Zienkiewicz, The Finite Element Method, 3rd Edn., McGraw-Hill, London (1977).

4. K. J. Bathe and A. P. Cimento, Some Practical Procedures for the solution of Nonlinear Finite Element Equations, Comput. Meths. Appl. Mech. and Engrg., 22, 59-85, (1980).

5. P. G. Bergan, G. Horrigmoe, B. Krakeland, and T. H. Soreide, Solution Techniques for Nonlinear Finite Element Problems, Int. J. Numer. Methods Eng., 12, 1677-1696 (1978).

6. J. J. Dongarra, Performance of various computers using standard linear equations software in a Fortran environment, Mathematics and Computer Science Division, Argonne National Lab., Jan. 10, (1984).

7. J. J. Dongarra and S. C. Eisenstat, Squeezing the most out of an algorithm in Cray Fortran, Argonne National Lab., Tech. Memo. ANZ/MCS-TM-9, (1983).

8. V. R. Saunders and M. F. Guest, Applications of the Cray-1 for quantum chemistry calculations, Comput. Phys., 26, 389-395, (1982).

9. J. R. Rice, Elastic-plastic fracture mechanics, in The Mechanics of Fracture, ASME Winter Annual Meeting, New York, December, (1976).

10. J. R. Rice, A path independent integral and the approximate analysis of strain concentration by notches and cracks, J. Appl. Mech., 35, 379-386, (1968).

11. J. R. Rice and G. F. Rosengren, Plane strain deformation near a crack tip in a power law hardening material, J. Mech. Phys. Solids, 16,1-12, (1968).

12. J. W. Hutchinson, Singular behavior at the end of a tensile crack in a hardening material, J. Mech. Phys. Solids, 16, 13-31, (1968).

13. J. W. Hutchinson, Plastic stress and strain fields at a crack tip, J. Mech. Phys. Solids, 16, 337-347, (1968).

14. J. R. Rice, Mathematical analysis in the mechanics of fracture, in Fracture (edited by H. Liebowitz), Vol. 2, Mathematical Fundamentals, p. 191, Acadamic Press, New York, (1968).

15. D. M. Tracey, Finite elements solutions for crack-tip behavior in small scale yielding, Transactions ASME, J. Engineering Materials and Technology, 98, 146-151, (1976).

16. P. D. Hilton and J. W. Hutchinson, Plastic intensity factors for plates, Eng. Fract. Mech., 3, 435-451, (1971).

17. Y. Yamada, N. Yoshimura, and T. Sakurai, Plastic stress-strain matrix and its application for the solution of elastic-plastic problems by the finite element method, Int. J. Mech. Sci., 10, 343-354, (1968).

18. H. M. Van Rij and P. G. Hodge, Jr., A slip model for finite element plasticity , J. Appl. Mech., 45, 527-532, (1978).

19. P. G. Hodge, Jr. and H. M. Van Rij, A finite element model for plane strain plasticity, J. Appl. Mech., 46, 536-542, (1979).

20. J. G. Malone, Minnesota Supercomputer Institute Tech. Rep. (in preparation).

21. G. Yagawa, Y. Takahashi, and K. Kashima, Elastic-plastic analysis on stable crack growth for center cracked plate: a benchmark study, Eng . Fract. Mech., 19, 4, 755-769, (1984).

22. L. M. Kachanov, Foundations of the Theory of Plasticity, North-Holland, (1971).

23. S. K. Chan, I. S. Tuba, and W. K. Wilson, On the finite element method in linear fracture mechanics, Eng. Fract. Mech. , 2, 1-17, (1970).

24. P. J. Sydow, Cray computer systems technical note, Optimization Guide SN-0220,

Cray Research Inc., (1982)

25. I. Higbie, Vectorization and conversion of Fortran programs for the Cray-1 (CFT) compiler, Publication no. 2240207, Cray Research, Inc., (1979).

26. Cray-1 computer systems, Fortran (CFT) Reference Manual, Publication # SR-0009, Cray Research, Inc.

LIST OF TABLES AND FIGURES

mesh	M	N	number of elements	number of nodes	d. o. f.	r_1
A	49	3	1260	694	1319	1.0×10^{-6} a
B	33	3	876	486	919	1.0×10^{-4} a
C	19	3	564	304	569	5.6×10^{-3} a
D	34	6	2064	1098	2122	6.1×10^{-3} a

Table II. 1. Mesh parameters.

E_T (G Pa)	mesh	no. of iterations per load step at applied load f				total no. of load steps	average no. of elements yielded per step	total c. p. u. time (secs.)	average c. p. u. time per step (secs.)	d.o.f.
		0.07	0.3	0.6	0.9					
2.372	A	16	31	37	49	608	2.0	740	1.217	1319
2.372	B	18	32	35	51	425	2.0	416	0.979	919
18.510	A	10	14	17	19	510	2.4	338	0.663	1319
18.510	B	10	14	17	19	353	2.4	178	0.504	919
18.510	C	9	15	16	18	221	2.3	66	0.299	569
18.510	D	9	16	16	20	373	5.0	709	1.901	2122

Table II. 2. Computing times for both materials using different meshes (each program run is for a maximum applied load of f=0.98).

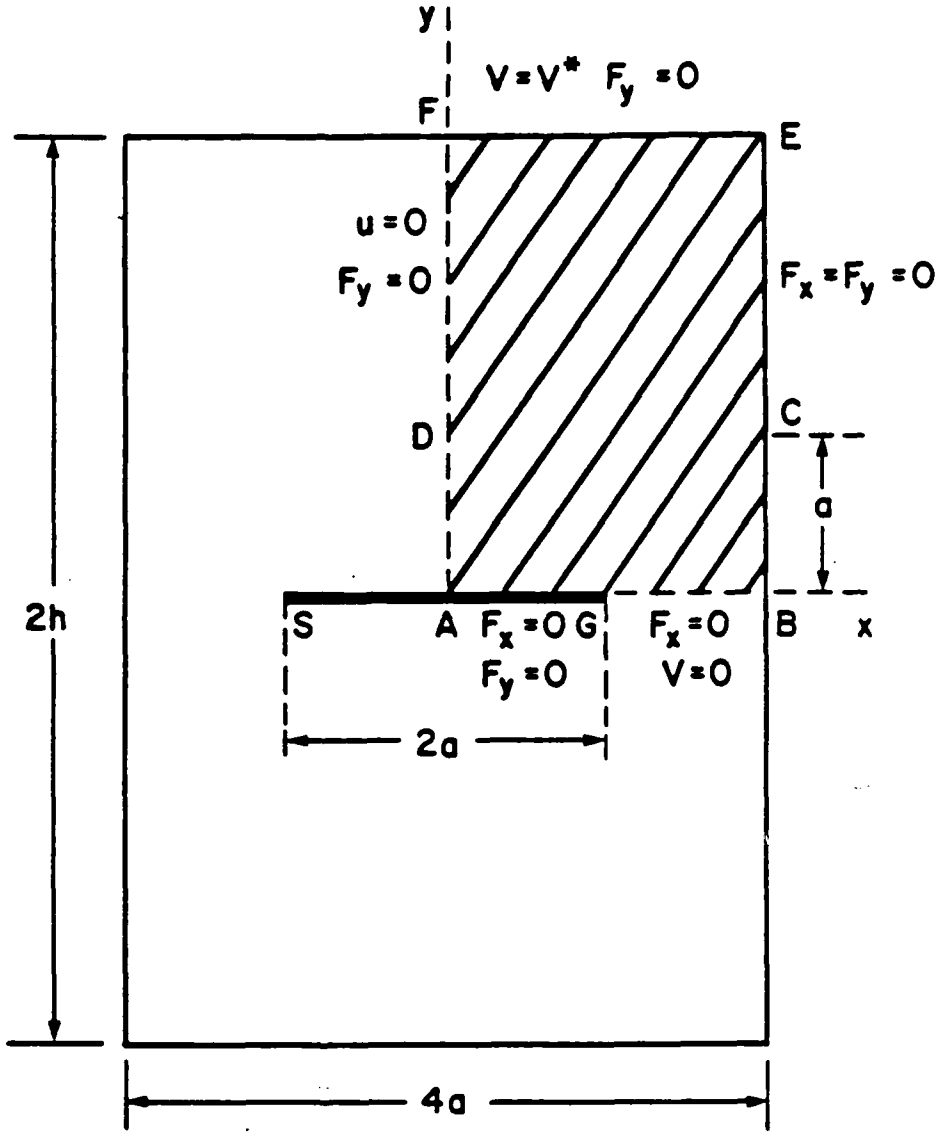

Figure II. 1. Center cracked plate.

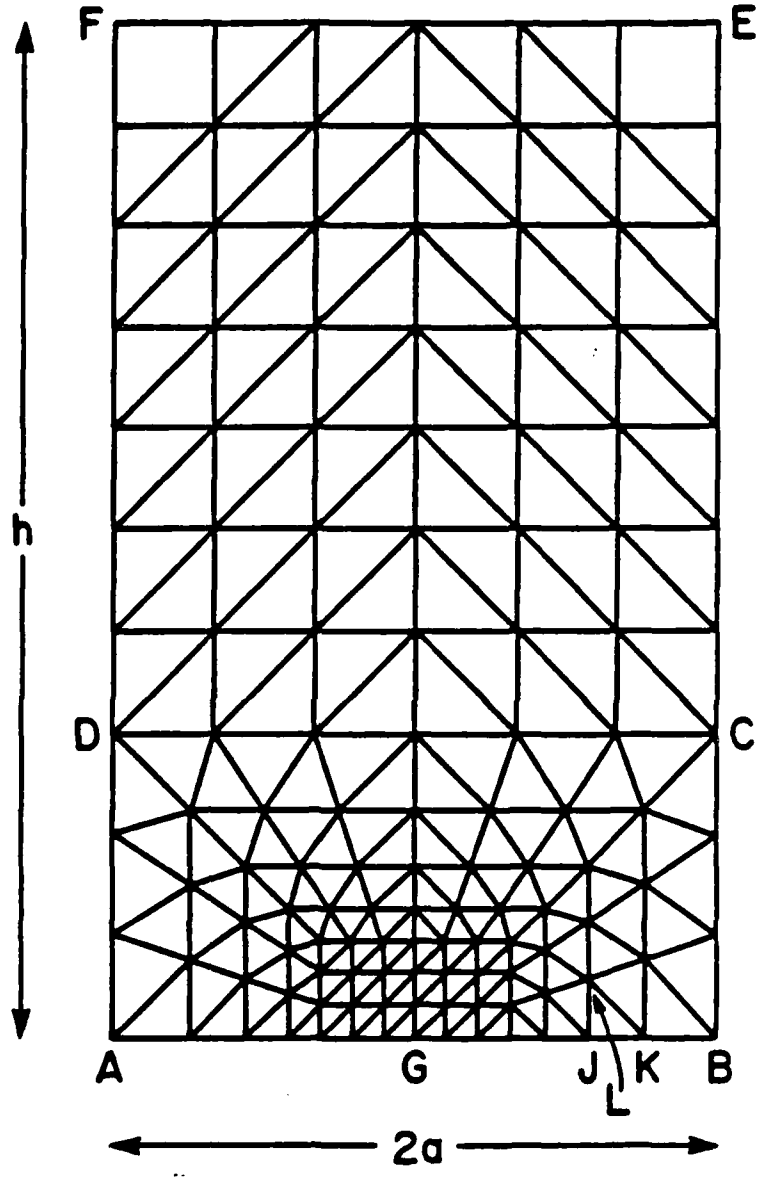

Figure II. 2. Typical mesh (M=5, N=3).

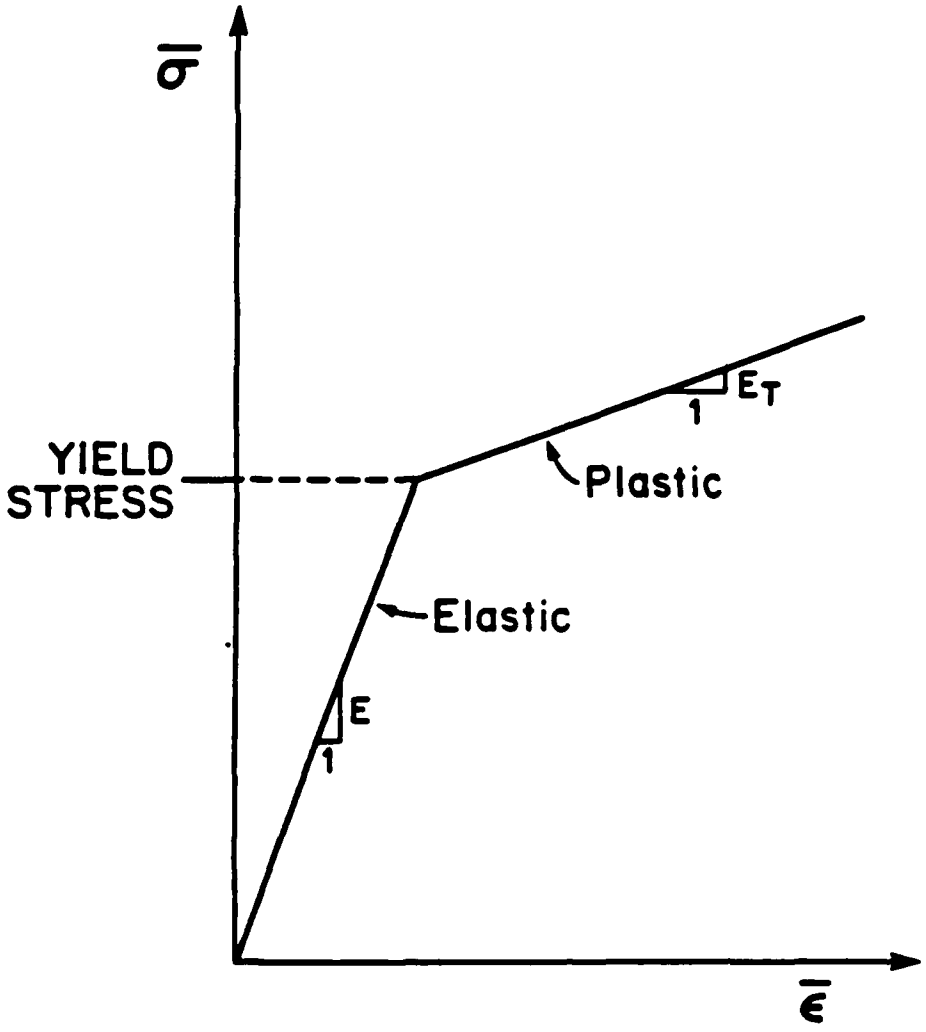

Figure II. 3. Equivalent stress vs. equivalent strain.

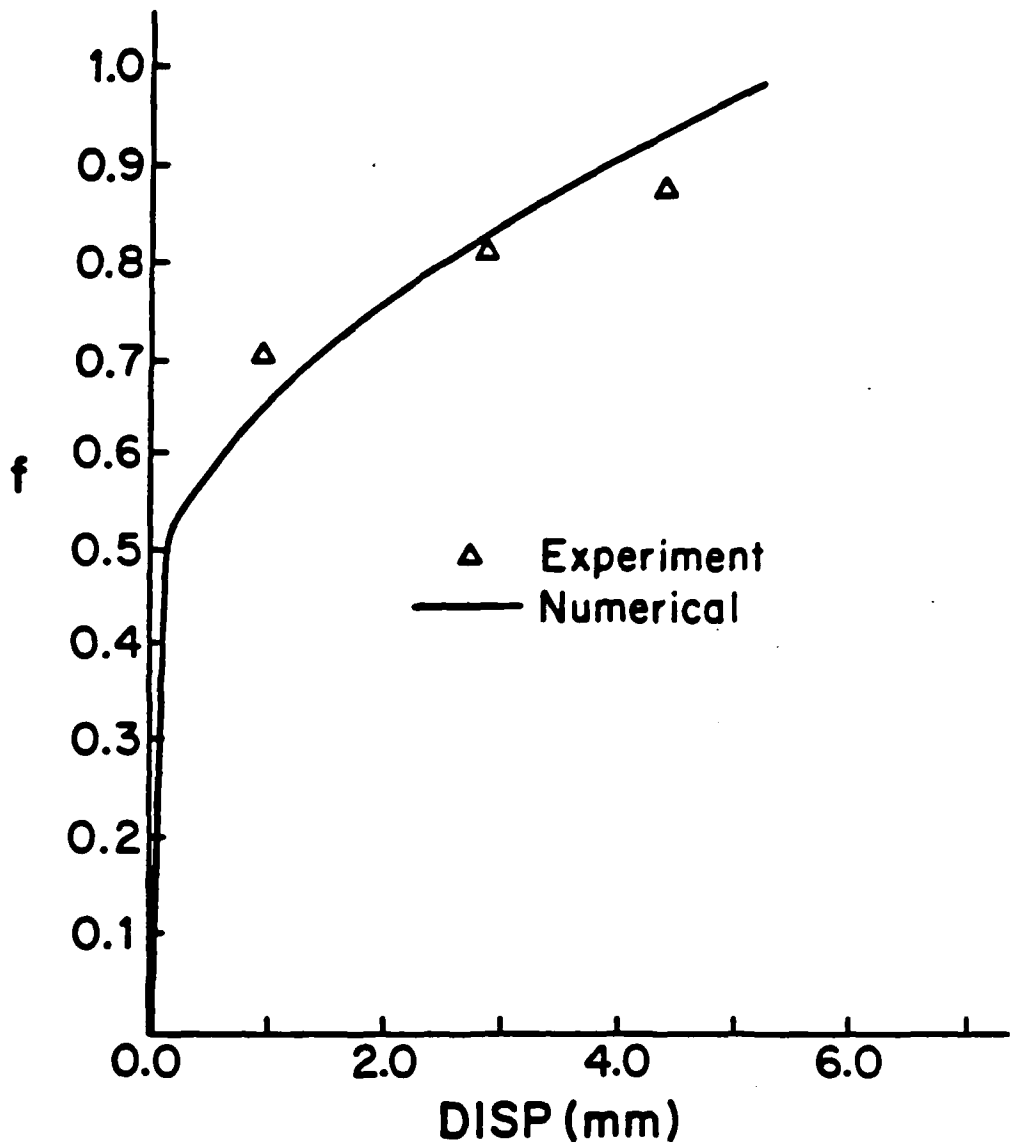

Figure II. 4. Load vs. gage point displacement.

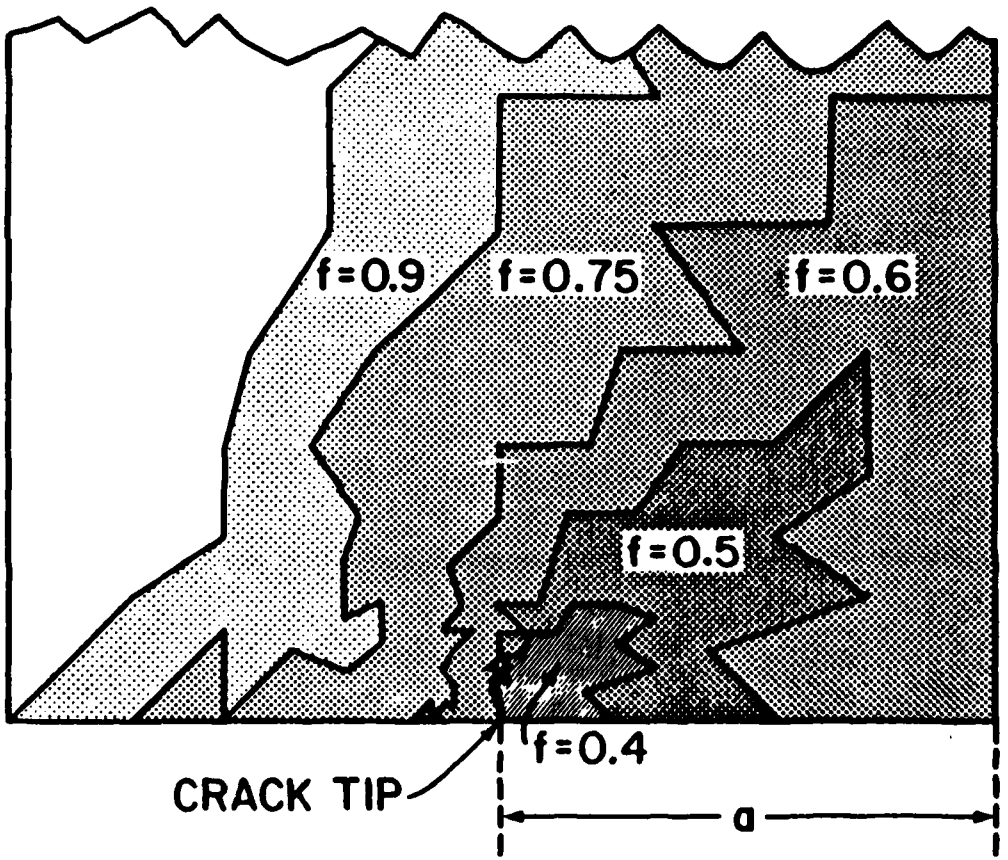

Figure II. 5. Growth of plastic zones.

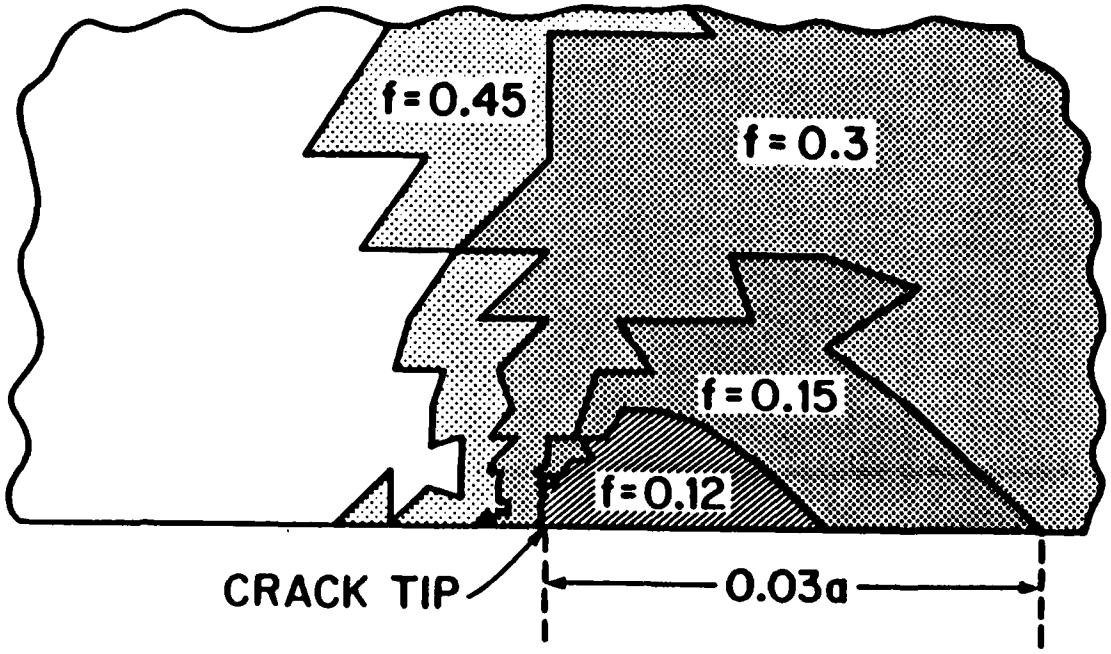

Figure II. 6. Growth of plastic zones near tip.

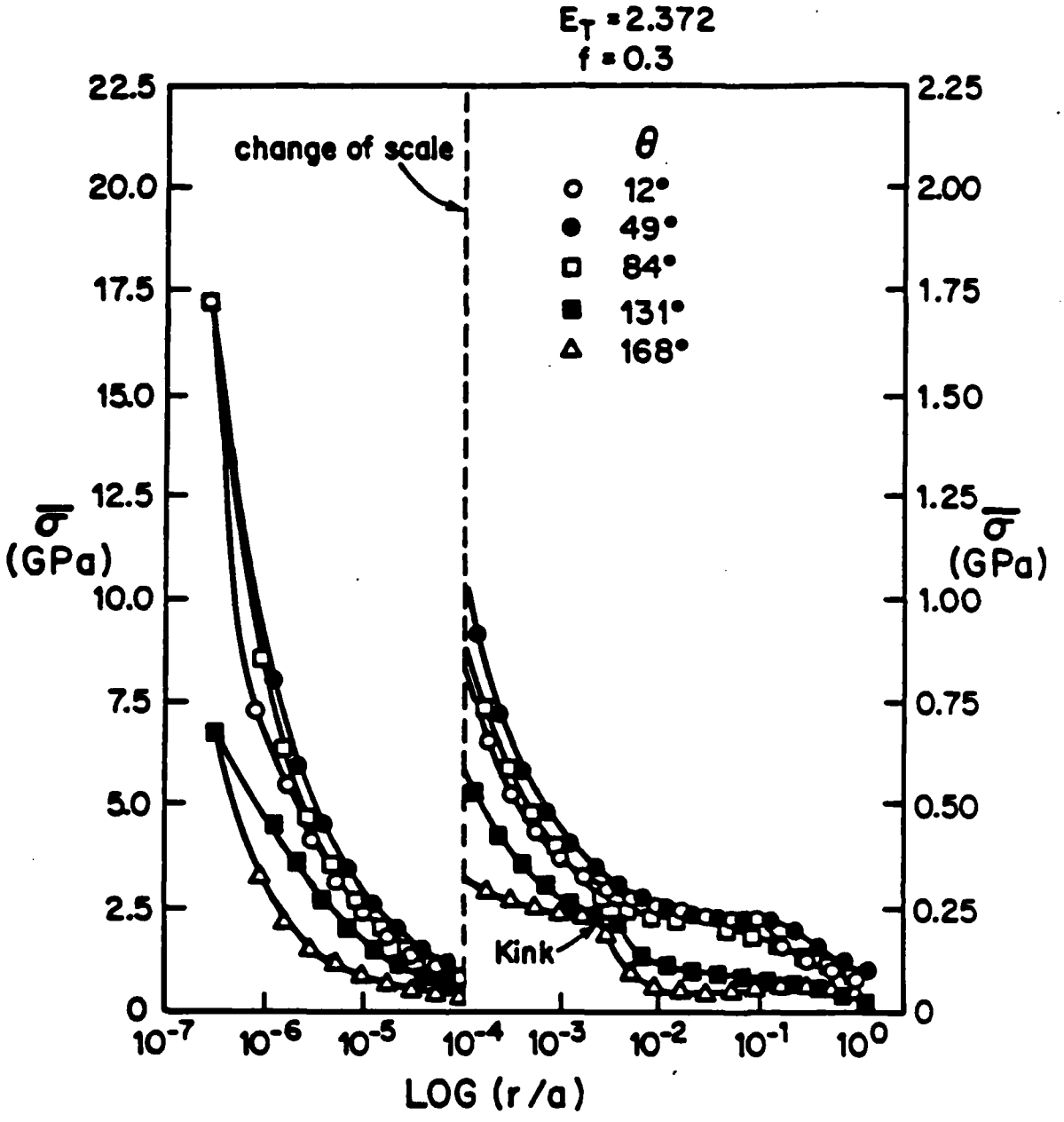

Figure II. 7. Equivalent stress field at an applied load of f= 0.3.

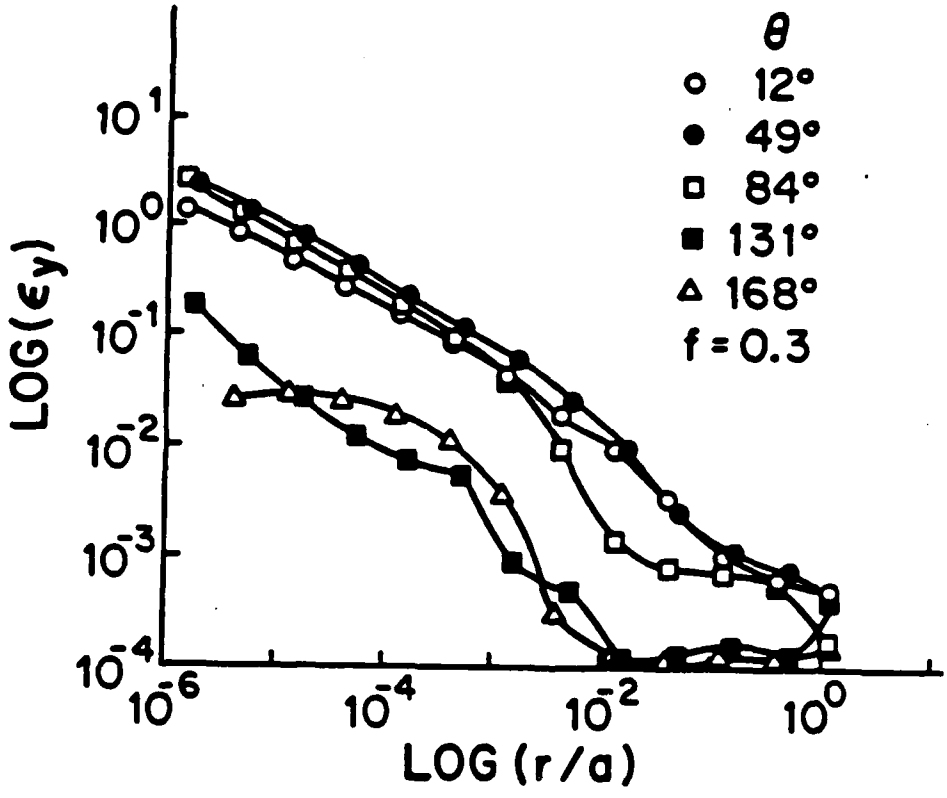

Figure II. 8. Strain field at an applied load of f=0.3.

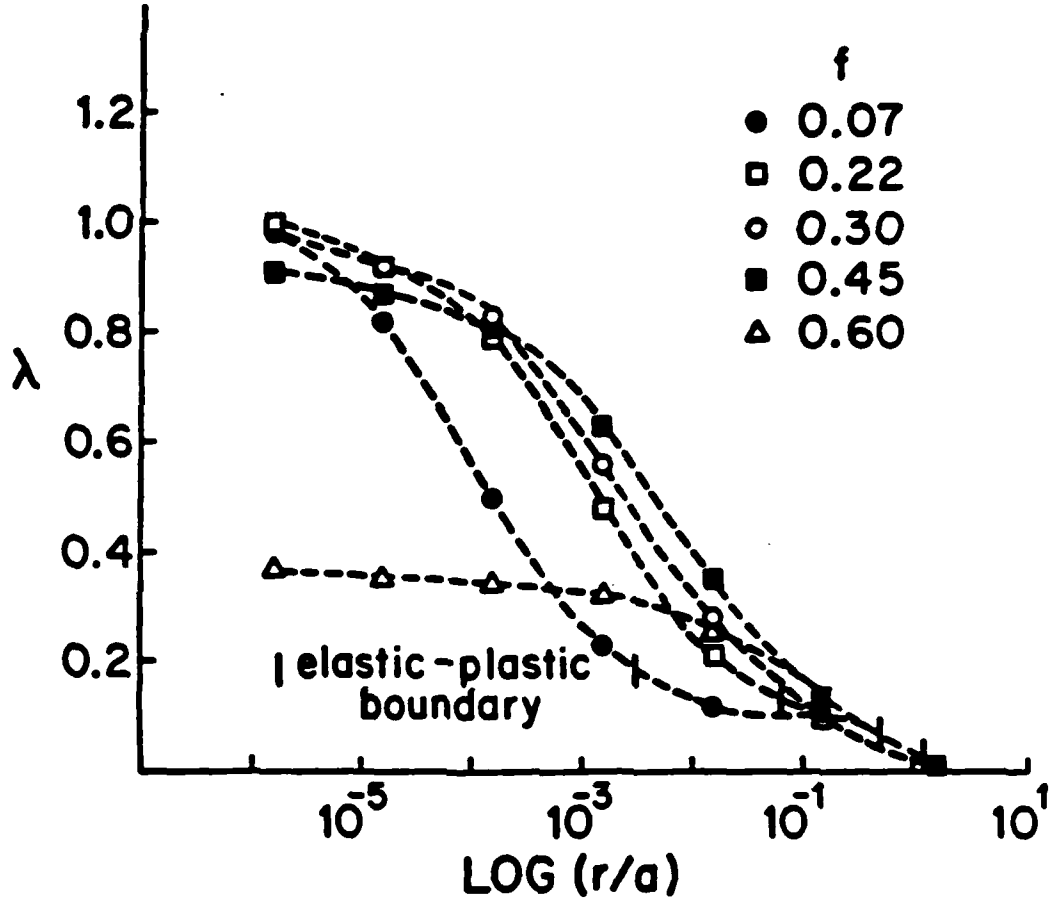

Figure II. 9. Comparison of HRR and finite element stresses along the 49 ^{0} ray.

END

DTIC

5-86